Hindawi
Advances in Civil Engineering
Volume 2020, Article ID 2760952, 17 pages
https://doi.org/10.1155/2020/2760952

Research Article

Experimental Study on Physicomechanical Properties of Deep Sandstone by Coupling of Dry-Wet Cycles and Acidic Environment

Xin Huang, Jianyong Pang, Guangcheng Liu, and Yu Chen

School of Civil Engineering and Architecture, Anhui University of Science and Technology, Huainan 232001, China

Correspondence should be addressed to Jianyong Pang; jypang@aust.edu.cn

Received 11 November 2019; Revised 18 December 2019; Accepted 18 January 2020; Published 21 March 2020

Academic Editor: Hugo Rodrigues

Underground engineering, especially deep geotechnical engineering, is often affected alternately by groundwater infiltration and ventilation drying during construction and use. In addition, acid rain, mineral dissolution, acid deposition, and other factors make groundwater acidic. This caused the underground structure to erode and has also threatened its safety and durability. In this study, both the physical and mechanical properties under acid dry-wet (A-D-W) cycles were investigated. Deep sandstone was treated repeatedly under acid cycling, and its physical parameters were measured. Uniaxial compressive strength tests and microtests were carried out. Finally, using a combination of scanning electron microscopy (SEM) and backscatter electron images (BSE), the microstructural changes of sandstone under the combined action of an acidic environment and a dry-wet cycle were described. The test results show that the mass, *P*-wave velocity, peak stress, and elastic modulus of sandstone after the A-D-W cycles decreased by 0.43%, 7.87%, 70.20%, and 88.10%, respectively. With the increase in the number of cycles, the loss of these indicators increased. However, the peak strain increased with an average increase of 55.8%. In addition, 10 cycles are the critical point for physical and mechanical indicators of the A-D-W cycles. After 10 cycles, the changes of various indicators increase rapidly. Microscopic analysis shows that the reasons of this phenomenon were that the specimen was corroded by the sulfuric acid solution, which resulted in the development of pores and cracks and the decline of physical and mechanical properties. Conversely, the development of pores was hindered by sediment, which slowed down the decline rate of the physical and mechanical indexes of specimens, but this phenomenon disappeared with the increase of A-D-W cycles. Based on the analysis of the experimental phenomena, the constitutive model of uniaxial compression based on *Weibull* damage variable has been established in this article, and the model has the best effect in acid solution with less cycle times or pH value of solution greater than 6.

1. Introduction

Water-rock interaction is an important driving force for the evolution of the near-surface environment. It has a great influence on the geological structure of the strata and the stability of underground engineering under the coupling action of chemistry and mechanics [1–4]. As one of the important forms of water-rock interaction, dry-wet cycling studies the effects of water on the physical and mechanical properties of rocks by simulating periodic changes of water content. In recent years, sufficient research works have been done on the variation of static rock mechanical parameters under dry-wet cycling [5–8]. The results show that the dry-wet cycling has an obvious deterioration effect on the basic mechanical properties of rock, such as compressive strength, elastic modulus, cohesion, and the internal friction angle. Currently, the study of the variation of mechanical parameters of rock materials under a dynamic environment is becoming more and more abundant, Zhou et al. [9] found that the dynamic compressive strength and elastic modulus of sandstone decreased with the increase of the number of dry-wet cycles, and the empirical equation of the effect of the strain rate and dry-wet cycles on the dynamic compressive strength of the rock materials was established through experiments. Du et al. [10, 11] found that the dynamic compressive strength of red sandstone was positively correlated with the loading rate and negatively correlated with the number of dry-wet cycles.

The attenuation function model was established to evaluate the dynamic compressive strength of red sandstone under the influence of dry-wet cycles, whereas the constitutive model was developed for the coupling condition of impact load and dry-wet cycles. With the advancement of research, the testing range of mechanical parameters extends to tensile strength [12], shear properties [13, 14], and fracture characteristics [15]. With the development of microtechnology and the leap of detection technology, scanning electron microscopy (SEM) [16], nuclear magnetic resonance (NMR) [17], computed tomography (CT) [17], and acoustic emission (AE) [18] technologies are now often used to study the microchanges of rocks under dry-wet cycles.

In addition, due to acid rain, mineral dissolution, acid deposition, and other factors, the groundwater is acidic. The investigation of the rock damage law under the coupling action of the chemical solution and the dry-wet cycles is still in its initial stage. Because of the difference in chemical solutions, the experimental results will be slightly different, but the general law is consistent. Li et al. [19, 20] studied the variation of calcareous sandstone in an acid solution, and the chemical reaction rate was used to describe the degree of rock corrosion. The corresponding chemical damage model was established. Liu et al. [21–26] took the sandstone in the ebb-flow zone of a reservoir in the Three Gorges as the research object. They summarized the changing law of mechanical properties and macro- and microdamage mechanisms of sandstone under dry-wet cycles [21, 22] as well as the change of the physical parameters and microdamage mechanisms of limestone under chemical solution immersion. They found that the basic reason for the decline of the mechanical properties of rocks was that the pH value of the chemical solution changed the porosity and microdamage evolution of the rocks [23]. In addition, they also analyzed the deterioration rule of sandstone mechanical parameters under acid-base conditions [24, 25] and developed a numerical simulation program based on an improved Duncan–Chang constitutive model [26]. Matsumoto et al. [27] found that the dissolution of some substances in rocks can promote the development of cracks and that physical and chemical weathering promote each other and jointly accelerate rock failure. Sun and Zhang [28] used a magnesium sulfate solution to treat sandstone specimens by dry-wet cycles.

The results show that 30 cycles is the threshold of the physical and mechanical parameters of sandstone. They pointed out that color lightness and thermal conductivity can effectively evaluate the tensile strength of sandstone. Li et al. [29] investigated the effects of acid solution immersion on the physical and mechanical properties of sandstone. It was found that the deformation characteristics of sandstone under immersion in an acid solution such as sulfuric acid were softening, and the softening degree was positively correlated with the immersion time. Based on the experimental results, the damage constitutive model of sandstone under an acid ring was established. In addition, Fang et al. [30] studied the failure mechanism of the rock mass under the action of dry-wet cycling from the micromorphological change of joint surface. His research found that the dry-wet cycling made the roughness coefficient of the rock surface, the compressive strength of the face wall, and the basic friction angle gradually decrease, which led to a decrease in the shear strength of the joint surface. Yang et al. [31] studied the influence of water-rock cycles on the macro- and microproperties of rocks.

Macroscopically, the uniaxial mechanical properties of the water-rock cycle decrease progressively and continuously. Microscopically, the grain size characteristics and pore distribution of the rock surface gradually increase. To simulate more extreme environments, Ni et al. [32] carried out dry-wet-freezing-weathering simulation tests on the distribution of two sandstones. It was found that water content and salt solution treatment have a great influence on rock properties. Although salt solution can alleviate rock weathering, the specific mechanism needs to be studied. Zhang et al. [33] treated expansive rocks by dry-wet cycling and studied the law of crack propagation. The results show that the expansibility of expansive rocks decreases with the dry-wet cycling, which shows that the degree of cracking, fractal dimension, and the strength of expansive rocks decrease. Hu et al. [34] studied the crack development mechanism of mudstone under dry-wet cycling. Expansion during drying resulted in the increase of crack width and the decrease of crack size due to the entry of water. However, the penetration area of water increased with the number of dry-wet cycles, which led to the rapid increase in crack number and accelerated the fracture process of the mudstone. All of the studies show that the repeated processes of dry expansion and wetting compaction of different rock masses are characterized by strength reduction and crack increase. However, the different water solutions and the change in wetting and drying cycles lead to a change of rock properties, and therefore, the wetting and drying cycles under specific conditions are still worthy of further study.

The construction of underground engineering in a coal mine is an example of typical deep underground engineering. The surrounding rock of the coal mine roadway is under high geostress for a long time. When disturbed by excavation, it usually produces expansion or deformation, which is in the state of dry-wet circulation under the combined action of roadway ventilation and acid groundwater infiltration. In this article, the sandstone with a buried depth of −965 m is processed into specimens. After soaking in a sulfuric acid solution with pH values of 4 to 7 for five days, the sandstone is dried and wetted 0, 5, 10, and 15 times, respectively, and uniaxial compressive strength tests and microtests are then carried out to study the change rules of the physical, mechanical, and the evolution process of the microstructure. Based on the test, the uniaxial damage model of the sandstones were established, and its applicability and accuracy were evaluated.

2. Materials and Methods

2.1. Specimen Preparation. Sandstone specimens were collected from a roadway with a depth of −965 m in the Huainan mining area, Anhui Province, China (see Figure 1(a)). The roadway has been affected by groundwater infiltration for a

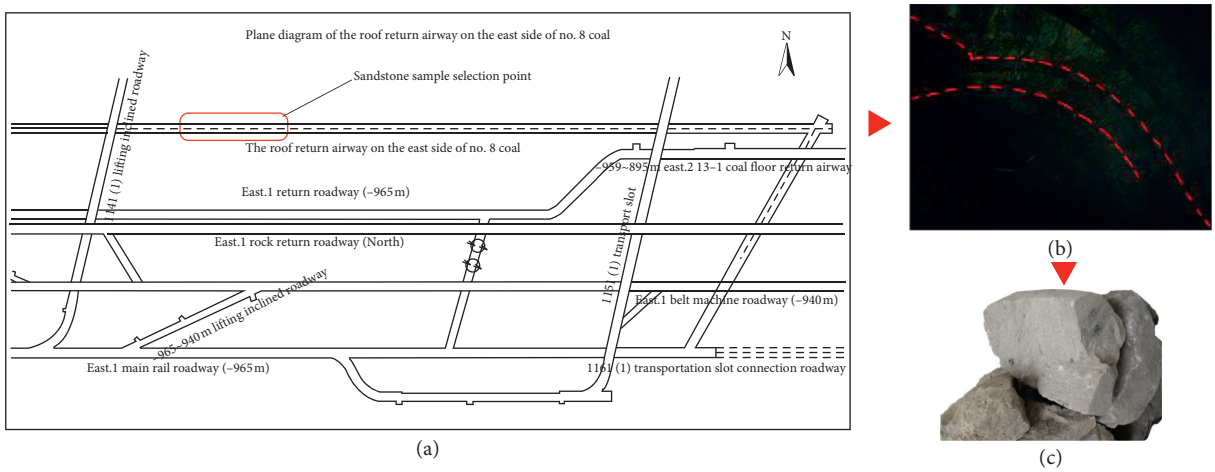

Figure 1: Sandstone specimens selection location: (a) plane diagram of the roof return airway on the east of the no. 8 coal, (b) roadway real scene, and (c) appearance of the rock specimen.

long time. The surrounding rock of the roadway roof has expanded, and the U-shaped steel support has deformed (see Figure 1(b)). The apparent characteristics of the rock specimens are grey-white, with a few dark brown spots (see Figure 1(c)).

According to the results of the X-ray diffraction (XRD) spectrum (see Figure 2(a)) and energy dispersive spectrometer (EDS) analysis, the main components of the specimens are quartz, albite, calcite, kaolinite, and iron compounds. The EDAX Octane plus spectrometer (see Figure 3(c)) was used to analyze the two detection points on the specimen surface (see Figure 2(b)).

The types of material elements on the surface of the specimens (see Figures 2(c) and 2(d)) and the results of the mass ratio analysis are shown in Table 1.

Combined with Figures 2(b)–2(d), it can be seen that the surface of the specimens is relatively flat with a small number of white spots. Spots 1 and 2 were selected to analyze the types of elements and their mass ratios, and the relative number of elements was calculated according to the relative atomic mass (see Table 1). It can be seen that the brighter the color, the more the types of elements, and the number of elements and relative atoms are in accord with the XRD results. It is proven that the matrix is mainly quartz (SiO_2). The speckles are metal element compounds and cementing materials (such as Fe_2O_3 and MgO). The metal element compounds are mainly Fe-containing compounds, and dark red spots can be observed on the surface of the macroscopic specimens.

In order to better understand the mineral composition, particle size, and structure of the rocks, specimens were taken and the thin sections were identified. Thin sections of rock with length × width × thickness of 30 mm × 20 mm × 0.03 mm were prepared by grinding. The thin sections were observed under a Leitz-ORTHOPLAN polarizing microscope in Germany (see Figure 4). The results show that the quartz content is 70%, the clay mineral is 15%, the siliceous rock is 10%, and the feldspar is 5%. The scattered distribution of quartz can be observed on the thin slices. The filler consists of muddy impurities and a small amount of biotite and kaolinite.

Specimens were selected based on similar *P*-wave velocities and made into cylindrical specimens with a diameter of 50 mm and height of 100 mm according to the ISRM (International Society for Rock Mechanics) standard [35]. The surface smoothness was controlled to within ±0.05 mm and the vertical deviation between upper and lower surfaces was controlled to within ±0.25 (see Figure 5).

The basic physical parameters of the prepared specimens were measured and the results are shown in Table 2.

2.2. Test Equipment. The mass of the sandstone specimens was measured by an electronic balance with an accuracy of 0.01 g and the *P*-wave velocity was measured by a nonmetallic ultrasonic testing analyzer of the NN-4B type. Drying and wetting cycles were dried in a 101-00 constant-temperature drying oven and immersed in a glass box. The uniaxial compression test used a WAW-2000 microcomputer-controlled electro-hydraulic servo universal testing machine with a maximum range of 2000 kN. The testing device is shown in Figure 3(a). In this experiment, the XRD (X-ray diffraction) instrument was a SmartLab high-resolution X-ray diffraction instrument (see Figure 3(b)), and the SEM (scanning electron microscope), BSE (back-scattered electron Imaging), and EDS (energy-dispersive spectrometer) were done using a Hitachi S-3400N scanning electron microscope (see Figure 3(c)).

2.3. Test Method

2.3.1. Solution Preparation. Solutions with pH of 4, 5, and 6 were prepared with concentrated H_2SO_4 and the solution with pH = 7 was prepared with tap water. Each solution measured 12 L.

2.3.2. The A-D-W Cycle Mechanism. The grouping method was as follows: the 48 specimens were divided into four

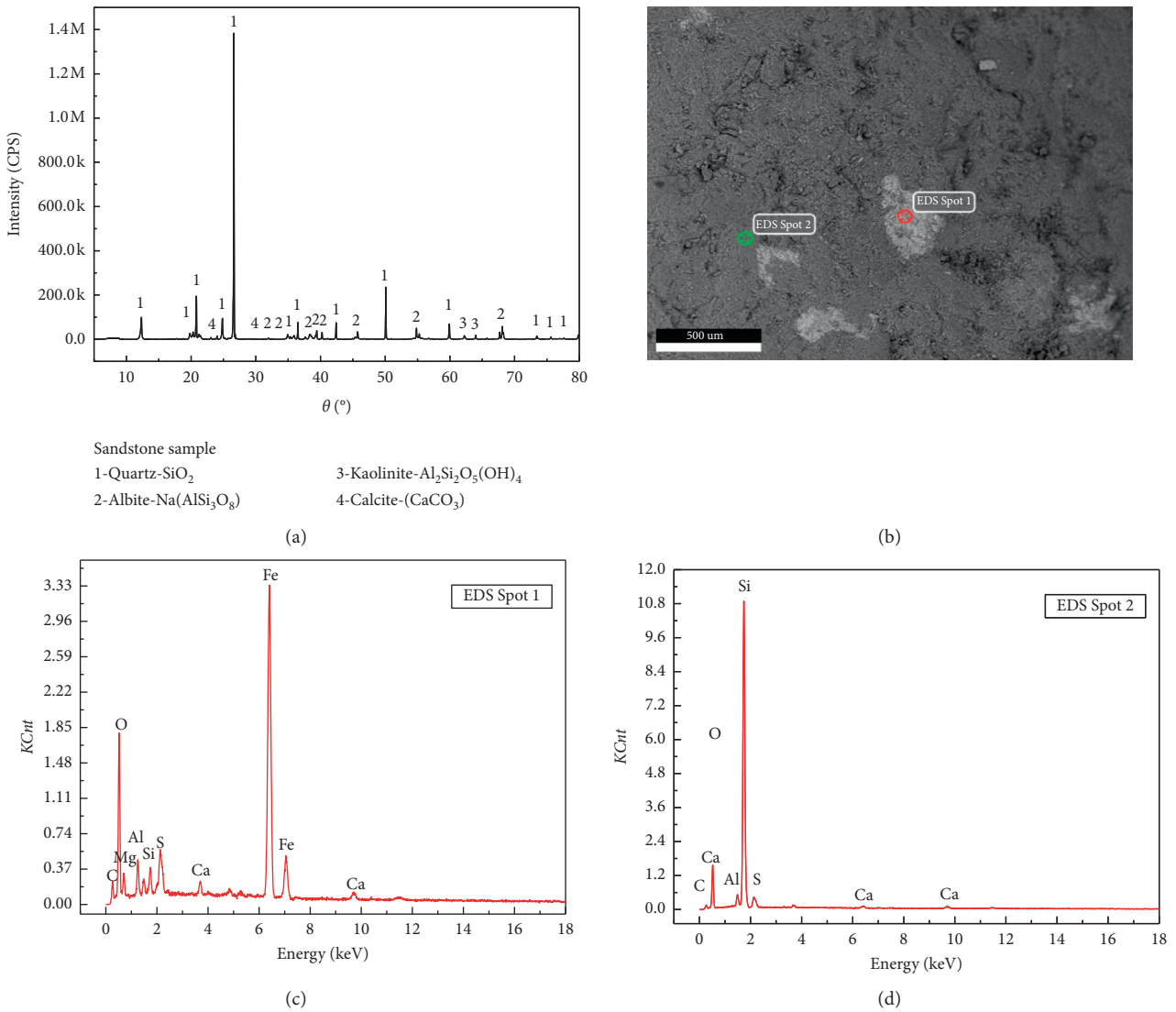

Figure 2: XRD and EDS observation of sandstone: (a) XRD spectrum (15°C), (b) EDS spots (15°C, 500 μm), (c) Spot1 element analysis, and (d) Spot 2 element analysis.

Figure 3: Partial test instrument: (a) WAW-2000 Universal Testing Machine, (b) SmartLab 18 KW, and (c) Hitachi S-3400N.

Table 1: EDS analysis results.

EDS Spot 1			EDS Spot 2		
Element types	Weight (%)	Relative atomic number	Element types	Weight (%)	Relative atomic number
C	11.16	9.7	C	13.40	10.9
O	36.33	22.7	O	42.01	26.3
Mg	5.67	2.3	Al	1.26	0.4
Al	1.06	0.4	Si	40.73	14.5
Si	1.26	0.4	S	2.39	0.7
S	2.07	0.6	Ca	0.21	<0.1
Ca	0.38	<0.1	—	—	
Fe	42.07	7.5	—	—	

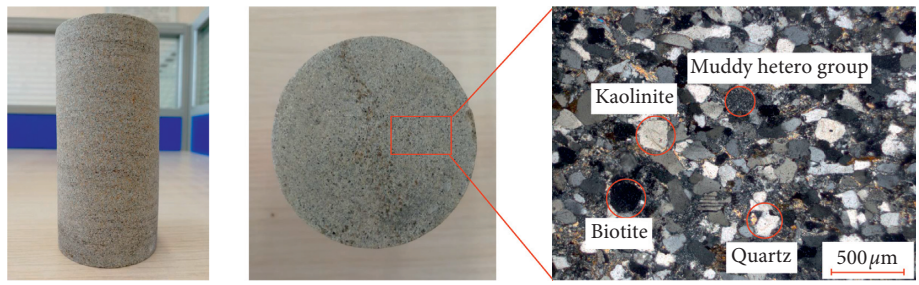

Figure 4: Test results of thin sections of rock specimens (a) rock specimens and (b) Identification results of thin sections.

Table 2: Average of basic physical parameters of sandstone specimens.

Physical parameters	Average mass (g)	Natural density (kg/m^3)	Drying density (kg/m^3)	Saturation density (kg/m^3)	Dry *P*-wave velocity (km/s)	Saturation *P*-wave velocity (km/s)
Value	506.21	2.496	2.477	2.642	4.523	4.774

Figure 5: Test sandstone specimens.

groups, which were soaked in the solutions with a pH of 4, 5, 6, and 7, respectively. Each group was further divided into four additional groups, which were then treated in four stages: stage I (5-day solution soaking), stage II (0–5 cycles), stage III (5–10 cycles), and stage IV (10–15 cycles).

According to the groupings, the specimens were treated by soaking them in different pH solutions for 12 hours, and then drying them in the drying oven for 12 hours, which was regarded as a dry-wet cycle. The first drying temperature of the drying oven was set to 105°C, and then each temperature was maintained at 60°C. The schematic diagram of the A-D-W cycle process is shown in Figure 6.

2.3.3. Uniaxial Compressive Strength Test Method. In the uniaxial test, the displacement control method was used to load the specimens, and the loading speed was 2 mm/min. To reduce the influence of the surface smoothness of the specimens on the test and to ensure the stability of the test instrument, all specimens were preloaded at the beginning of the test, and the preload was 500 N.

2.3.4. Microscopic Test Method. In order to compare the microstructural changes of the specimens experiencing different A-D-W cycles, four groups of specimens in stages I-IV were selected for microtesting at pH = 4. The micro-evolution process of the specimens was observed by SEM and BSE images.

3. Results and Discussion

3.1. Variation in Mass. During the coupling process of the acid solution and the wet-dry cycle, the acid solution immersion will dissolve some substances in the sandstone or react with the acid solution. On the other hand, the specimen

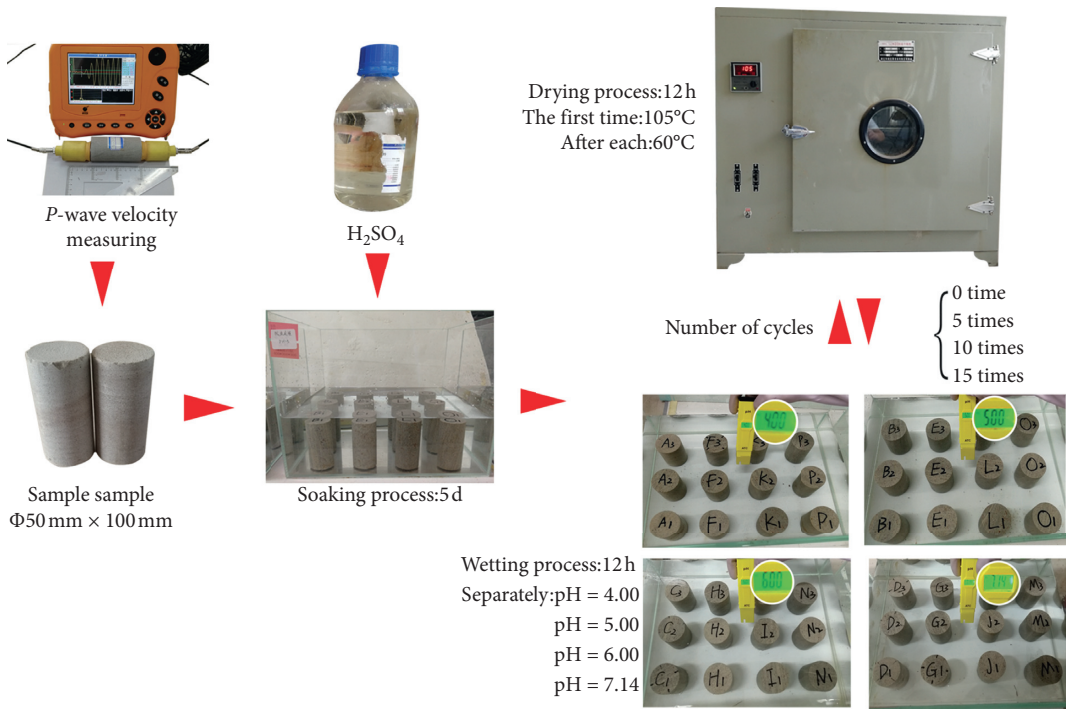

Figure 6: A-D-W cycle process.

surface may be peeled off repeatedly due to wet-dry alternation, resulting in a decrease of specimen mass. Therefore, the variation of the sandstone mass is an important index of the influence of the A-D-W cycle on sandstone damage. Table 3 records the average mass change of each group of sandstone specimens after completion of different A-D-W cycles.

In Figure 7, the curve corresponds to the left coordinate axis and the column diagram corresponds to the right coordinate axis. The changes in total mass loss and stage mass loss of sandstone specimens in different pH solutions are shown It can be seen from the variation of the curve that when pH = 4, the mass loss gradually increases to 0.17%, 0.21%, 0.31%, and 0.43% with the progress of the cycle. By comparing different curves, it can be seen that the mass loss increases with the decrease of pH value. Taking the test group with pH = 4 as an example, the proportions of the mass loss in each stage to total loss are 40.4%, 22.9%, 8.7%, and 28.0%, respectively. It can be seen that the mass loss increases obviously in Stage IV. This is because the sulfuric acid solution and the calcium ions dissolved in the specimen will form gypsum ($CaSO_4$), which has a certain inhibitory effect on the crack development of sandstone specimens with higher integrity. After 10 cycles, the crack development is complete, the inhibitory effect is weakened, so the internal material of the specimen continues to peel off and the decline in quality increases again.

The pH value of the acidic solution has a significant effect on the total mass loss of specimens. With the decrease in pH, the mass loss values are 1.05 g, 1.38 g, 1.74 g, and 2.18 g, respectively. It can be observed that the mass loss of the

Table 3: Variation of sandstone specimen mass under different conditions.

Stage of A-D-W cycle	pH = 4 Mass (g)	pH = 5 Mass (g)	pH = 6 Mass (g)	pH = 7 Mass (g)
Natural state	506.67	524.91	516.70	505.56
Stage I	505.79	524.24	516.11	505.13
Stage II	505.60	524.06	515.96	504.98
Stage III	505.10	523.76	515.71	504.76
Stage IV	504.49	523.17	515.32	504.51

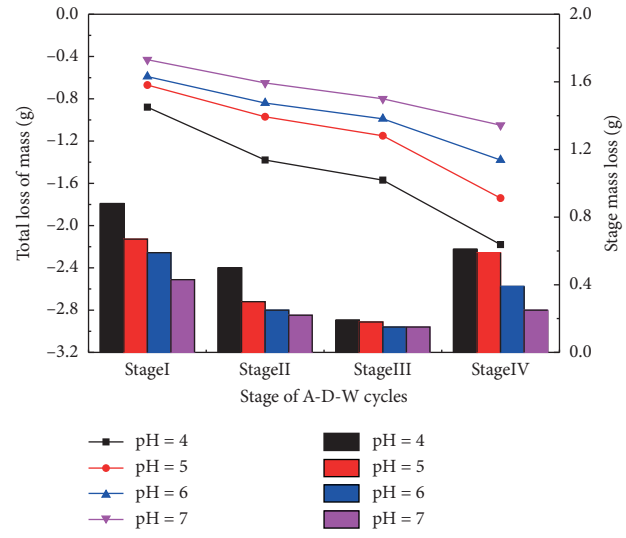

Figure 7: Changes of average mass loss of specimens versus solutions pH and A-D-W cycles.

specimens increases with the increase in acid concentration at the same wet-dry cycle stage, and the difference becomes more obvious with the increase in cycle times.

3.2. Variation of P-Wave Velocity. *P*-wave velocity is an important index for measuring the compactness of a material. The higher the velocity, the higher the compactness of the sandstone. Ultrasound travels faster in solids than in air, and gas-solid coupling leads to low average velocity. This indirectly indicates the cracks and pores in the specimen. The rock integrity coefficient k is introduced to describe the degree of development of rock fractures, and the k value is expressed as shown in

$$k = \left(\frac{V_m}{V_r}\right)^2, \quad (1)$$

where V_m is the initial *P*-wave velocity of the specimen, m/s and V_r is the *P*-wave velocity of the specimen after different dry-wet cycles, m/s. The calculation results are shown in Table 4.

The smaller the k value in Table 4 indicates the poorer the rock integrity. It can be seen that with the increase of the number of dry-wet cycles, the k value of the specimen decreases gradually. At the same time, with the decrease of the pH value, the integrity of the sandstone specimen also decreases. The specific decline rule is shown in Figure 8.

In Figure 8, the curve corresponds to the left coordinate axis and the column diagram corresponds to the right coordinate axis. The variation of the total loss of *P*-wave velocity and stage loss of *P*-wave velocity of sandstone specimens in different pH solutions are shown.

It can be seen from the curve that the *P*-wave velocity of each group of specimens shows a downward trend with the progress of the A-D-W cycle. The most obvious decrease is at pH = 4, where the total decrease in *P*-wave velocity at each stage is 2.20%, 3.14%, 5.16%, and 7.87%, respectively. In addition, it can be seen from the column diagram that the *P*-wave velocity losses at stages I and II are equivalent, which is different from the law of continuous decline in mass loss analysis. This is because the ultrasonic wave is mainly emitted along the axis of the specimen during the *P*-wave velocity measurement, and the main measuring range is close to the center of the specimen. The spalling damage at the edge of the surface of the specimen has little effect on its interior. Also, it can be seen that the loss at stage IV is significantly higher than that of the first three stages, which agrees with the observation that the loss at stage IV increases sharply after 10 cycles found in Section 3.1.

3.3. Stress-Strain Curve. From the test results, the stress-strain curves of the treated and untreated specimens are drawn. The test curves of the treated specimens at stages I, II, III, and IV under different pH values are shown in Figure 9(a–d).

The typical $\sigma - \varepsilon$ curves of the A-D-W cycle for each group of specimens show the following. (1) The peak stress of specimens experiencing the A-D-W cycle is significantly lower than that of untreated specimens, and with the increase of cycling stage, the decrease of stress increases gradually. (2) The slope of the experiencing curve, the elastic modulus, also decreases with the increase of the cyclic stage. (3) Figures 9(a)–9(d) show that with the increase of the acid concentration, the peak strain increases gradually, and the more the cyclic stages are, the more obvious the phenomenon is.

According to the $\sigma - \varepsilon$ curve, it is easy to get the σ (peak stress) and ε (peak strain) of sandstone under different states. The E (elastic modulus) of sandstone under different states can be calculated by fitting the slope of the curve in the straight line before the curve reaches the peak stress. Its data are recorded as shown in Table 5.

Table 4: Variation of k value of sandstone specimen under different conditions.

Stage of A-W-D cycles	pH = 4 k	pH = 5 k	pH = 6 k	pH = 7 k
Stage I	0.960	0.970	0.974	0.983
Stage II	0.938	0.953	0.965	0.974
Stage III	0.899	0.923	0.935	0.953
Stage IV	0.849	0.886	0.905	0.924

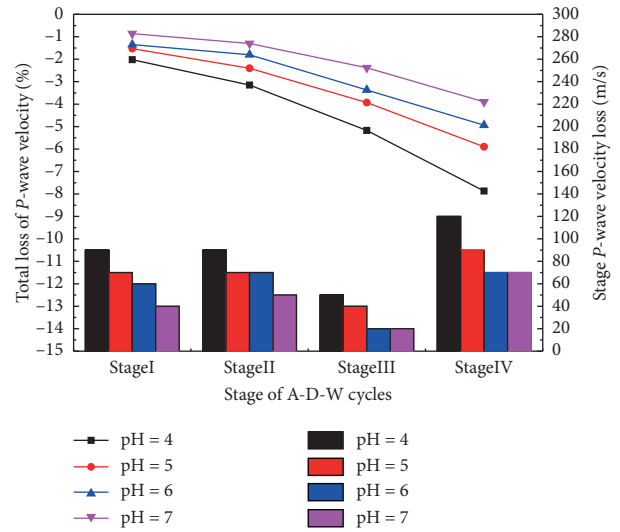

Figure 8: Changes of average *P*-wave velocity loss of specimens versus solution pH and A-D-W cycle.

3.3.1. Peak Stress. The results shown in Figure 10(a) show that compared with the peak stress of 97.96 MPa in the control group, after 15 times of A-D-W cycles, the percent decrease in stress are 53.2%, 64.40%, 70.3%, and 70.2% with the increase in acid concentration. At the same pH value, pH = 5, the peak stress loss for stages I to IV at different cyclic stages can be found to be 29.68 MPa, 28.02 MPa, 2.89 MPa, and 8.30 MPa, respectively. The corresponding stress loss of specimens is 30.46 MPa, 19.20 MPa, 3.54 MPa, and 10.91 MPa at pH = 6. Two sets of data show that the loss of peak stress in each stage decreases gradually in the first three stages of the cycles and increases again in Stage IV.

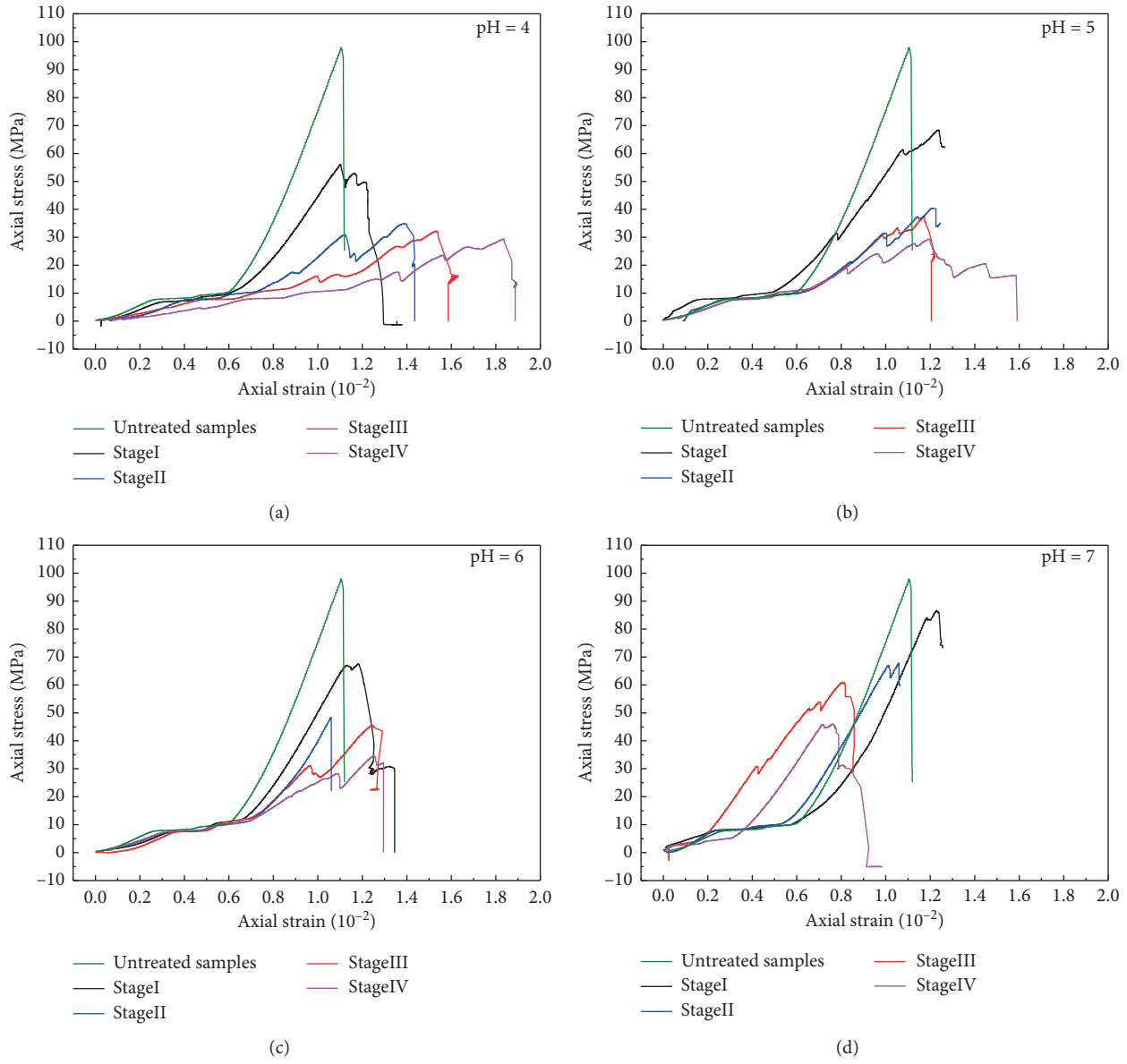

Figure 9: Stress-strain curve of sandstone specimens after A-D-W cycle: (a) pH = 4 group, (b) pH = 5 group, (c) pH = 6 group, and (d) pH = 7 group.

Table 5: Mechanical parameters of sandstone specimens under various conditions.

Stage of A-D-W cycles	Before immersion			pH = 4			pH = 5			pH = 6			pH = 7		
	σ (MPa)	E (GPa)	ε (‰)	σ (MPa)	E (GPa)	ε (‰)	σ (MPa)	E (GPa)	ε (‰)	σ (MPa)	E (GPa)	ε (‰)	σ (MPa)	E (GPa)	ε (‰)
Stage I	97.96	20.75	11.04	56.03	11.29	10.99	68.28	11.15	12.30	67.50	13.19	11.80	86.46	16.94	12.30
Stage II	—	—	—	34.83	7.16	13.90	40.26	6.54	12.10	48.30	13.11	10.61	66.91	13.33	10.09
Stage III	—	—	—	31.99	3.36	15.36	37.37	4.81	11.70	44.74	7.39	12.55	60.79	8.23	8.08
Stage IV	—	—	—	29.15	2.46	18.27	29.07	3.21	11.99	33.83	4.02	12.49	45.80	11.42	7.10

3.3.2. Elastic Modulus. The results shown in Figure 10(b) show that as compared with the control group, the elastic modulus is 20.75 GPa. After 15 times of A-D-W cycles, the decreasing rates of the test group were 44.9%, 80.6%, 84.5%, and 88.1% for pH = 7, 6, 5, 4, respectively. The percent loss of the pH group is more than 80%, which is 1.80–1.96 times that of the neutral group. This shows that acidity has a significant effect on the elastic modulus of the specimens. When the pH value is the same, the elastic modulus of the specimens decreases continuously with the progression of cycles.

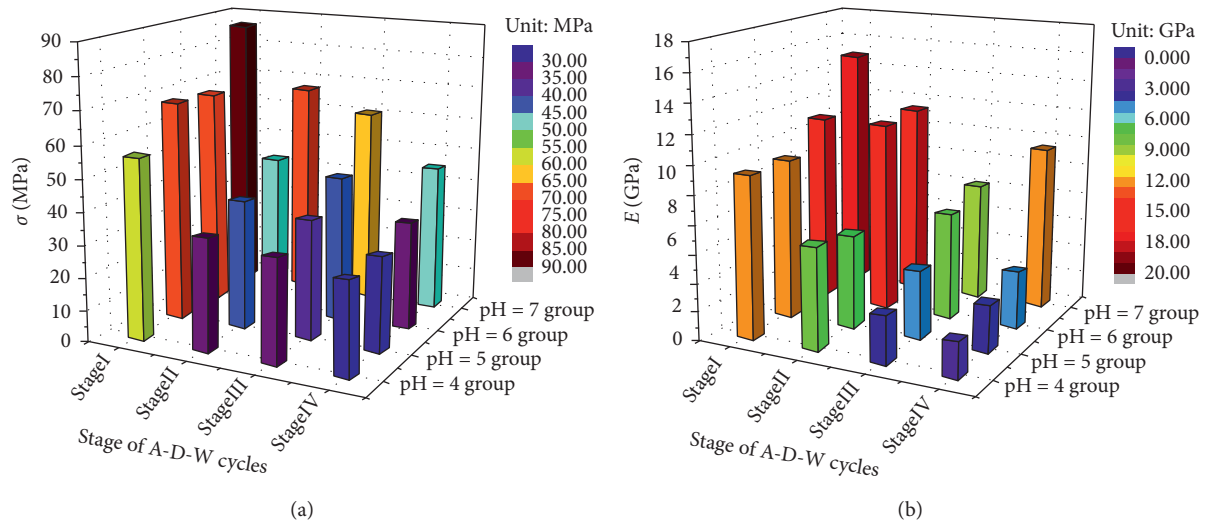

Figure 10: Effects of the A-D-W cycle on peak stress and elastic modulus under different groups: (a) relation of dynamic compressive strength under different stages and (b) relation of elastic modulus under different stages.

3.3.3. Peak Strain. The peak strain values of specimens with different pH groups at different cyclic stages are shown in Figure 11. In neutral solution, the peak strain of specimens decreases very gradually with the progression of cycles, which indicates that the brittleness of the specimens increases under normal dry-wet cycling conditions, and it is easier to produce sudden cracks leading to failure. However, with the addition of acidic solution, the peak stress of each group of specimens increases, which indicates that the acidic solution can soften the specimens and increase the ductility slightly, resulting in greater deformation and relatively mild failure mode. The average strain values of the different pH groups were also plotted. The results showed that the peak strain growth trend gradually slowed down from Stage I to Stage III, but by Stage IV, the total increase rate was 55.8%. The change rule also indicated that 10 cycles were the turning point for the physical and mechanical properties of the A-D-W cycle.

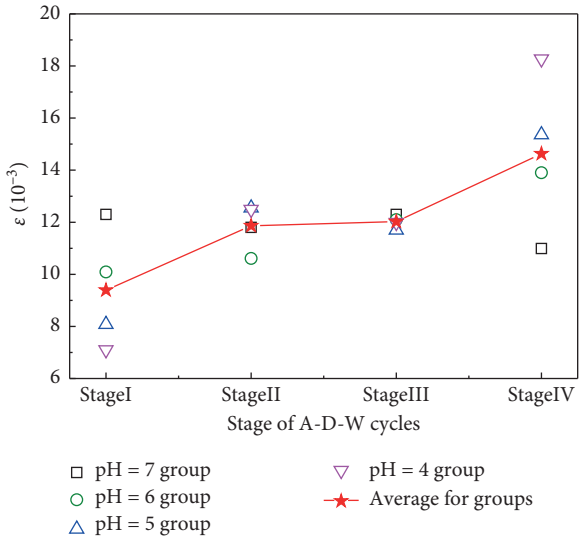

Figure 11: Variation of peak strain of sandstone versus A-D-W cycle.

3.4. Microstructure Evolution. Specimens from stages I–IV of the pH = 4 groups were collected. Scanning electron microscopy (SEM) was used to observe and obtain the microscopic morphology and structure of the specimens. The images obtained are shown in Figure 12. The SEM and BSE images of the specimens in the natural state are shown in Figure 13 as a control group for comparison.

In Figure 13, it can be observed that the surfaces of the sandstone specimens in the natural state are relatively flat and compact, there are no obvious cracks, and there are a few scattered natural pores; at this time, the peak stress and elastic modulus of the specimens are the maximum values of each group, and their integrity and mechanical properties are good.

The main reason for the decrease of the mechanical parameters of the specimen during the dry-wet cycle is the development of pores and cracks, which will gradually reduce the strength and elastic modulus of the specimen. According to common sense, the corrosion of the acid solution will cause the development of cracks, and the expansion of the cracks in turn allows the acid solution to further enter the inside of the specimen. Under the repeated action of the dry-wet cycle, these two factors promote each other and accelerate the damage rate of the specimen. However, the test results show that the rate of decrease of the mechanical parameters of the specimen gradually decreases before 10 dry-wet cycles, and after 10 times, the specimen begins to deteriorate rapidly. It is found through the microstructure photography that the cause of this phenomenon is the development of pores or cracks affected. In the early stage of the dry-wet cycle, the surface of the specimen is dense, but the number of pores increased compared with Figure 13(a). The pores served as channels, which causes the acid solution to further corrode the inside of the specimen,

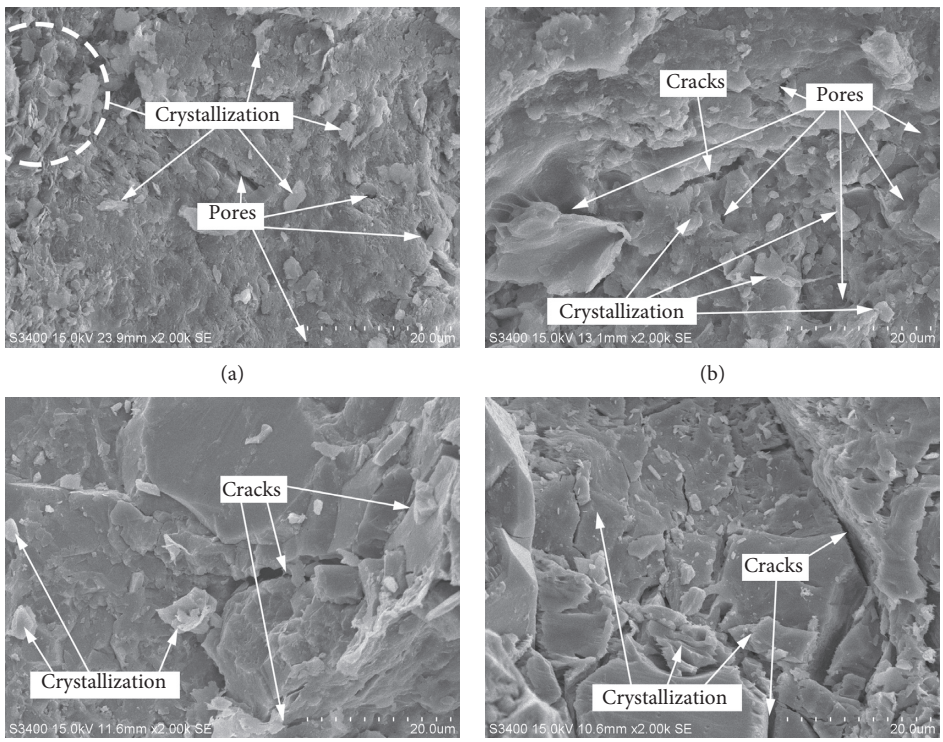

Figure 12: SEM image of specimens in different A-D-W cycle stages (at pH = 4): (a) Stage I, (b) Stage II, (c) Stage III, and (d) Stage IV.

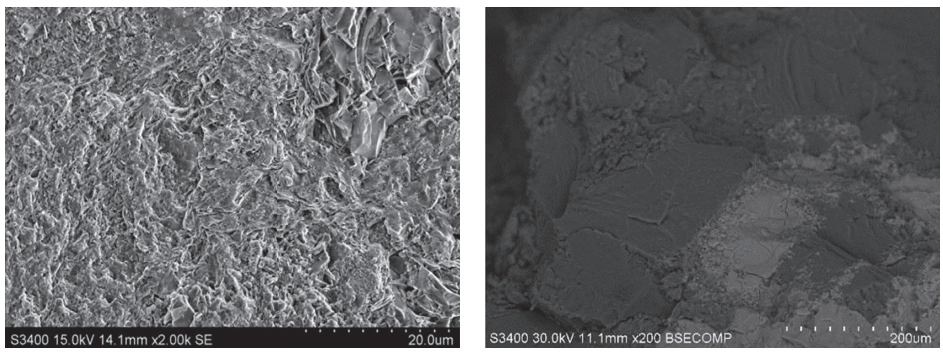

Figure 13: Microscopic image of sandstone in its natural state: (a) SEM image of specimens and (b) BSE image of sandstone.

causing the inside of the specimen to be damaged. The mechanical properties of the components are significantly reduced (see Figure 13(a)). As the cycle progresses (see Figure 12(b)), microcracks begin to develop, and the crystalline material gradually increases. When the specimen is under pressure, the cracks start to grow from the microcracks and promote the failure of the specimen. Mechanical parameters continue to decline. However, in Figure 12(c), we find that new precipitation occurs, which adheres to the surface of the specimen to a certain extent, hindering the entry of the acidic solution, forcing the acidic solution to react with the precipitated material, and then further accelerate the crack development. As a result, the rate of decline of the macro-mechanical parameters of the specimen is slowed down, but the amount of precipitation is limited after all. As the dry-wet cycle progresses, this phenomenon gradually disappears. After 10 dry-wet cycles, cracks are distributed in the network and connected. Crystal materials begin to gradually decrease (see Figure 12(d)), the macro-mechanical properties of the sample further deteriorated, and the rate of decline of the mechanical parameters of the specimen increased again.

In order to further observe the process of crack development, the surface of the specimen was ground and flattened, and a back-scattering electron (BSE) image of 200 μm was taken (Figure 14).

Figure 14(a) shows that the surface of the specimens is compact, the pores are small, most of them are in the

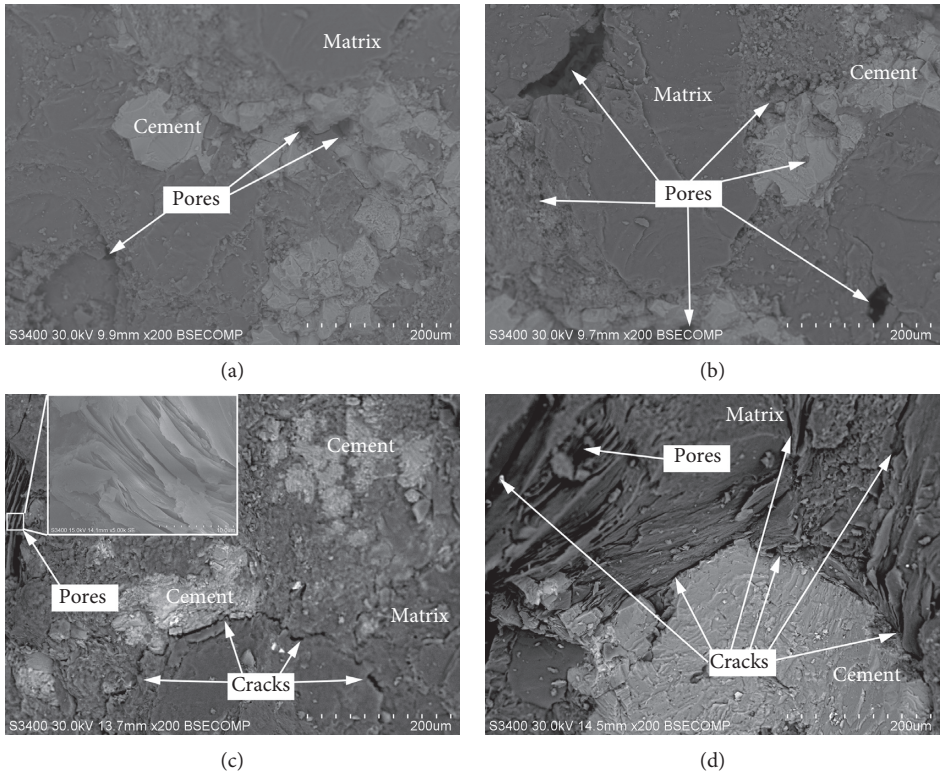

Figure 14: BSE image of specimens in different A-D-W cycle stages (at pH = 4): (a) Stage I, (b) Stage II, (c) Stage III, and (d) Stage IV.

cementing materials, and the matrix is relatively complete. With the enlargement of the pore area, new fine pores continue to appear on types of cement (see Figure 14(b)). Figure 14(c) shows that fissures first appear at the interface between the matrix and the cement, and the matrix in the original pore begins to curl in layers under the corrosion of the acidic substances. The cracks further develop and prolong, and microcracks begin to appear in the matrix. The matrix curling range in the pore is enlarged and the degree of curling is deepened, which results in the decrease of the strength of specimens at the macroscopic level (see Figure 14(d)).

The coal mine sandstone used in this test is mainly composed of quartz, albite, kaolinite, and calcite. According to the change of microstructure, the XRD diffraction patterns (see Figure 15) of the specimens before and after the test show that the main substances on the surface of the specimens are still quartz and feldspar, while kaolinite and calcite have disappeared, and new products, calcium silicate and gypsum, have appeared. It is inferred that the main ion reactions are as in Figure 15:

Quartz is almost insoluble in an acidic environment, so acidic solution has little influence on it. Albite ($NaAlSi_3O_8$) reacts with H^+ in an acidic environment to form Na^+, Al^{3+}, and the precipitate orthosilicic acid (H_2SiO_4). The specific reaction equation is as follows:

$$NaAlSi_3O_8 + 4H^+ + 4H_2O = 3H_4SiO_4\downarrow + Na^+ + Al^{3+}. \quad (2)$$

The specific reaction equation of kaolinite ($Al_2Si_2O_5(OH)_4$) with acid is given by:

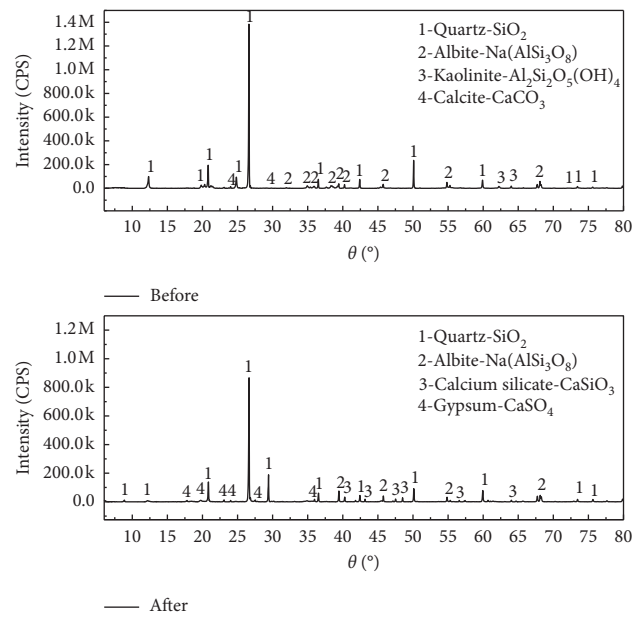

Figure 15: XRD diffraction pattern of specimen surface before and after test.

$$Al_2Si_2O_5(OH)_4 + 6H^+ = 2Al^{3+} + 2H_2SiO_3\downarrow + 3H_2O. \quad (3)$$

and the specific reaction equation of calcite ($CaCO_3$) with acid is as follows:

$$CaCO_3 + 2H^+ = Ca^{2+} + H_2O + CO_2\uparrow. \quad (4)$$

Reaction of metal compounds with acid solution is as follows:

$$\begin{aligned} Fe_2O_3 + 6H^+ &= 2Fe^{3+} + H_2O \\ MgO + 2H^+ &= Mg^{2+} + H_2O \end{aligned} \quad (5)$$

Fe^{3+} causes the solution to be reddish brown after immersion.

In addition, the free Ca^{2+} ion binds with the SO_4^{2-} ion to form gypsum ($CaSO_4$), and free Ca^{2+} ion binds with the SiO_3^{2-} ion to form calcium silicate ($CaSiO_3$), which are attached to the surface of the specimen with the original silicic acid (H_2SiO_4) and the silicic acid (H_2SiO_3). In the early stages of the A-D-W cycles, these substances can hinder the development of pores and slow down the damage rate of the physical and mechanical parameters. However, the structure and strength of the new substances are greatly different from those of sandstone, which ultimately leads to the failure of the specimen:

$$\begin{aligned} Ca^{2+} + SO_4^{2-} &= CaSO_4\downarrow \\ Ca^{2+} + SiO_3^{2-} &= CaSiO_3\downarrow \end{aligned} \quad (6)$$

3.5. Damage Mechanism Analysis. The failure mechanism of sandstone in the acidic environment can be summarized by combining the microstructure evolution process of the specimens with the failure morphology of the macrospecimens as shown in Figure 16.

The effects of the acidic solutions on sandstone include physical, such as lubrication, softening, mudding, and strengthening of bound water; chemical, which includes ion exchange, dissolution, hydration, hydrolysis, redox, precipitation; and mechanical, including pore hydrostatic pressure and pore hydrodynamic pressure, effects.

3.5.1. Water Lubricates Sandstone. Lubrication occurs when water enters the structural planes such as cracks, joints, and fault planes of the sandstone. It reduces the friction resistance and enhances the shear stress effect of the structural plane. This results in the shear failure of the specimens after multiple dry-wet cycles, which is reflected in the reduction of the internal friction angle in the macrosense.

3.5.2. Chemical Damage. The influence of the chemical solution of H_2SO_4 as the main acidic substance on sandstone includes two aspects. The acidic solution reacts with mineral particles, which reduces the size of the mineral particles and changes the size and shape of the rock particles. This results in changes in the size and shape of the pores and cracks (see Figure 16(a)). But, as this happens, the sulfuric acid solution changes the mineral composition of the rocks. Gypsum ($CaSO_4$) formed by the combination of SO_4^{2-} and Ca^{2+} in solution, albite ($NaAlSi_3O_8$), and kaolinite ($Al_2Si_2O_5(OH)_4$) form orthosilicic acid and silicic acid in the acidic environment. These products can adhere to the pore of the specimen when the crack is small, and change the porosity, which prevents further reaction between the acid solution and the internal sandstone to a certain extent (see Figure 16(b)). As the number of cycles increases, the mixture dissolves and breaks down (see Figure 16(c)). Cracks develop further, and the acid solution promotes the development of cracks, which lead to the failure of the specimens (Figure 16(d)).

3.5.3. Effect of Pore Water Pressure. Because of the acid dry-wet cycling process, the pore passages in the specimens are opened and the water content of the rock mass rises. Under the high geostress environment, the pore water in the specimen cannot be eliminated. Because of the water wedge effect, it promotes the propagation of the crack tip, thus roughly destroying the rock.

4. Establishment of Uniaxial Damage Model

4.1. Constitutive Equation of Sandstone under Uniaxial Compression. Generally, sandstone is a brittle material, which has three stages in uniaxial compression, i.e., compaction stage, linear elastic stage, and failure stage. Because of the complexity of the change law of the compaction stage and the sudden change of the failure stage, it is difficult to summarize its change law. Therefore, the uniaxial constitutive equation of sandstone is mainly the linear elastic stage. Its constitutive equation is shown as follows:

$$\sigma = E\varepsilon, \quad (7)$$

where σ is uniaxial compression stress value, MPa; E is modulus of elasticity, GPa; and ε is uniaxial strain value, 10^{-2}.

4.2. Damage Constitutive Equation of Sandstone under Uniaxial Compression in the A-D-W Cycles

4.2.1. Determination of Weibull Damage Variable. *Weibull* distribution [36] is used to describe the strength change of sandstone under the A-D-W cycles, and its probability density function is as follows:

$$p(x) = \frac{m}{F}\left(\frac{x}{F}\right)^{m-1} \exp\left(-\left(\frac{x}{F}\right)^m\right). \quad (8)$$

The cumulative probability of distribution is as follows:

$$P(x) = 1 - \exp\left(-\left(\frac{x}{F}\right)^m\right), \quad (9)$$

where m and F represent the inherent properties of rock materials [37].

From the microscopic point of view, the damage of rock material is caused by the damage of microunit structure in rock. It is assumed that for the specimens after n times of cycle, the number of microunits damaged under a certain load is c, the total number of microunits is N, and the statistical damage variable is defined as D.

$$D = \frac{c}{N}. \quad (10)$$

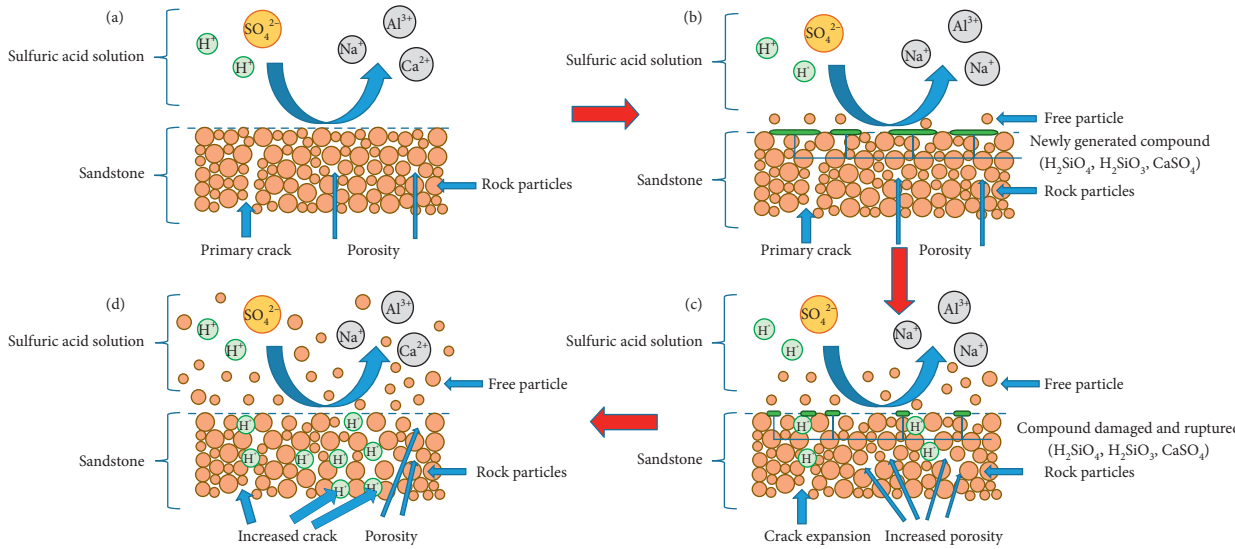

Figure 16: Sandstone damage mechanism: (a) Stage I, (b) Stage II, (c) Stage III, (d) and Stage IV.

During the $[\varepsilon, \varepsilon + d\varepsilon]$, the number of broken microunits is $Np(x)$, and then,

$$c(\varepsilon) = \int_0^{\varepsilon} Np(x)\mathrm{d}x = \left(1 - \exp\left(-\left(\frac{\varepsilon}{F}\right)^m\right)\right)N. \tag{11}$$

Joint (10) and (11) calculations.

$$D = 1 - \exp\left(-\left(\frac{\varepsilon}{F}\right)^m\right). \tag{12}$$

When $D = 0$, it means that the rock is undamaged; when $D = 1$, it means that all microunits are invalid; the size of D value indicates the degree of damage in the rock, $D \in [0, 1]$.

The uniaxial damage constitutive model of sandstone with damage variable is shown as follows:

$$\sigma = E\varepsilon(1 - D). \tag{13}$$

4.2.2. Calculation of Weibull Damage Variable Parameters. The damage constitutive model parameters F and m of rock under uniaxial compression can be calculated by the coordinate $C(\varepsilon_c, \sigma_c)$ of the peak point on the uniaxial stress-strain curve. When the stress-strain curve reaches the peak value, the slope of the curve is 0, and equation (14) can be obtained.

$$\left.\frac{\mathrm{d}\sigma}{\mathrm{d}\varepsilon}\right|_{\varepsilon=\varepsilon c} = \left[1 - m\left(\frac{\varepsilon_c}{F}\right)^m\right]\exp\left(-\left(\frac{\varepsilon_c}{F}\right)^m\right) = 0. \tag{14}$$

The coordinate of point C satisfies equation (13) and can be substituted into equation (14).

$$\sigma_c = E\varepsilon_c \exp\left(-\left(\frac{\varepsilon_c}{F}\right)^m\right). \tag{15}$$

Similarly for equations (10) and (11),

$$m = -\frac{1}{\ln\left(\sigma_c/E\varepsilon_c\right)}, \tag{16}$$

$$F = \varepsilon_c\left(\frac{1}{m}\right)^{-(1/m)}. \tag{17}$$

4.2.3. Determination of Damage Variables of A-D-W Cycle. The damage variable of acid dry wet cycle under uniaxial compression is defined as D_w,

$$D_w = 1 - \frac{E_n}{E_0}, \tag{18}$$

where E_n is the modulus of elasticity of n cycles under uniaxial compression, MPa; E_0 is the elastic modulus of 0 cycle under uniaxial compression, MPa.

According to the mechanical test results (see Table 5), it is assumed that the change of elastic modulus E with the number of A-D-W cycles n is continuous. Introducing fitting function $E_n = E_0[1 - K\ln(n^a + 1)]$, the change rule of elastic modulus under different pH values is fitted, and the results are shown in Figure 17.

4.2.4. Uniaxial Damage Constitutive Model of Sandstone under A-D-W Cycles. The uniaxial damage constitutive model of sandstone under different acid concentration is shown as follows:

$$\sigma = E_0\left[1 - K\ln\left(n^a + 1\right)\right]\varepsilon\exp\left(-\left(\frac{\varepsilon}{F}\right)^m\right), \tag{19}$$

Where σ is the strength of sandstone, MPa; ε is the strain of sandstone; E_0 is the elastic modulus of sandstone in its natural state, GPa; and K and a are the correlation coefficients of pH value. According to the fitting results in Table 6,

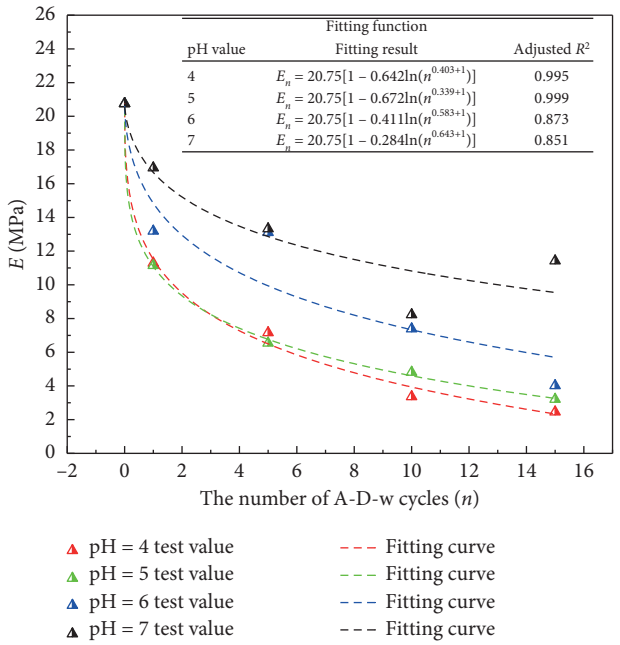

Figure 17: Fitting curve of E at different pH values.

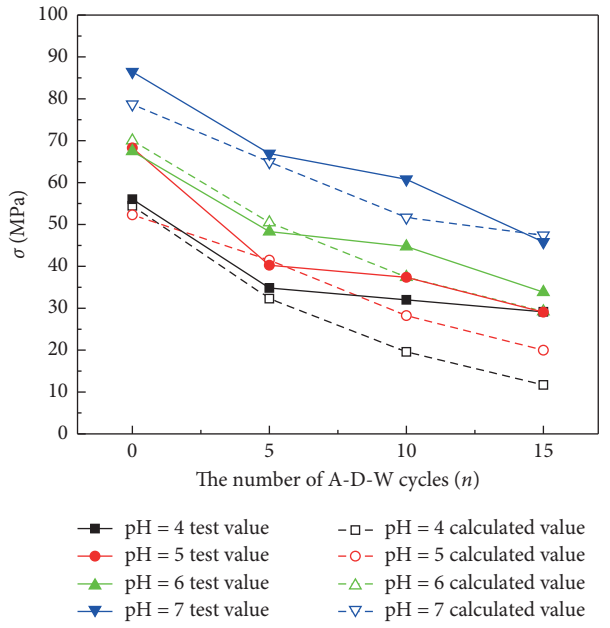

Figure 18: Relation of damage model value σ with n.

Table 6: Values of m and F in different states.

Parameter	Before immersion	pH = 4	pH = 5	pH = 6	pH = 7
m	1.177	1.258	1.434	1.197	1.137
$F/10^{-2}$	1.268	1.318	1.582	1.371	1.377

specific figures of this value can be obtained under different pH values; m and F are inherent properties of rock materials.

4.3. Verification of Sandstone Uniaxial Damage Constitutive Model. The inherent properties of rock are changed due to the specimen has been immersed in different solutions for 5 days (stage I). Therefore, the values of m and F of the soaked specimen are calculated according to formulas (16) and (17), as shown in Table 6. According to the constitutive model (19), the uniaxial mechanical parameters of sandstone are calculated and compared with the test values. The comparison results are shown in Figure 17.

The test value of stage I is calculated according to $m = 1.177$, $F = 1.268 \times 10^{-3}$ (before immersion). Because immersion changes the inherent properties of the specimens, when in stages II, III, and IV, the test values and calculation values of each group of specimens are as shown in Figure 18, according to the m, F values corresponding to different pH values.

The predicted value of damage model and test value are shown in Table 7.

4.4. Evaluation of Sandstone Uniaxial Damage Constitutive Model. As shown in Figure 18, when pH = 7, the predicted value of peak stress is exact. However, when the pH value is lower than 7 and the number of dry-wet cycles is more than 10, the predicted value of the specimen is lower than the test value. Therefore, the correlation coefficient R is used to evaluate the calculated value curve and the theoretical value curve, and the calculation formula is shown in equation (20) [38].

$$R = \frac{\sum_{i=1}^{n}(x_i - \overline{x})(y_i - \overline{y})}{\sqrt{\sum_{i=1}^{n}(x_i - \overline{x})^2 \cdot \sum_{i=1}^{n}(y_i - \overline{y})^2}}, \quad (20)$$

Where x and y, respectively, represent two groups of different variable values.

According to equation (20), calculate the correlation coefficient R between the peak stress test value and the calculated value of the specimen at different pH values, as shown in Table 8.

According to the R value of each experimental group in Table 8, the correlation coefficient of each group of specimens is greater than 0.8, showing a high correlation, indicating that the model prediction is accurate. Due to the cement produced on the surface of the specimen in the early stage of sulfuric acid solution (see Figure 14), further deterioration of the specimen is hindered to some extent, resulting in slightly higher test value than the predicted value.

According to equation (21), the relative error between the test value and the calculated value of each group of specimens is calculated.

$$W = \frac{|\sigma - \sigma_p|}{\sigma}, \quad (21)$$

Where W is the relative error, σ is the test value and σ_p is the calculated value. The calculation results are shown in Table 9.

According to the calculation results in the table, the larger the W value, the larger the deviation of the predicted value. When the pH value is greater than 6, the W value can be controlled below 0.2, which is more applicable. At the

Table 7: Comparison of calculated value and test value of damage model.

Stage of A-D-W cyces	pH = 4				pH = 5				pH = 6				pH = 7			
	σ (MPa)	E (GPa)	σ_p (MPa)	E_p (GPa)	σ (MPa)	E (GPa)	σ_p (MPa)	E_p (GPa)	σ (MPa)	E (GPa)	σ_p (MPa)	E_p (GPa)	σ (MPa)	E (GPa)	σ_p (MPa)	E_p (GPa)
	Test value		Predicted value		Test value		Predicted value		Test value		Predicted value		Test value		Predicted value	
Stage I	56.03	11.29	54.43	11.52	68.28	11.15	52.30	11.08	67.50	13.19	70.04	14.84	86.46	16.94	78.69	16.67
Stage II	34.83	7.16	32.29	6.51	40.26	6.54	41.47	6.77	48.30	13.11	50.48	9.93	66.91	13.33	64.91	12.86
Stage III	31.99	3.36	19.59	3.95	37.37	4.81	28.24	4.61	44.74	7.39	37.45	7.32	60.79	8.23	51.68	10.82
Stage IV	29.15	2.46	11.70	2.36	29.07	3.21	19.97	3.26	33.83	4.02	29.22	5.69	45.80	11.42	47.39	9.54

Table 8: Correlation coefficient R between test value and calculated value.

pH	4	5	6	7
R	0.96	0.91	0.98	0.96

Table 9: W value in different situations.

pH	4	5	6	7
Stage I	0.029	0.234	0.038	0.090
Stage II	0.073	0.030	0.045	0.030
Stage III	0.388	0.244	0.163	0.150
Stage IV	0.599	0.313	0.136	0.035

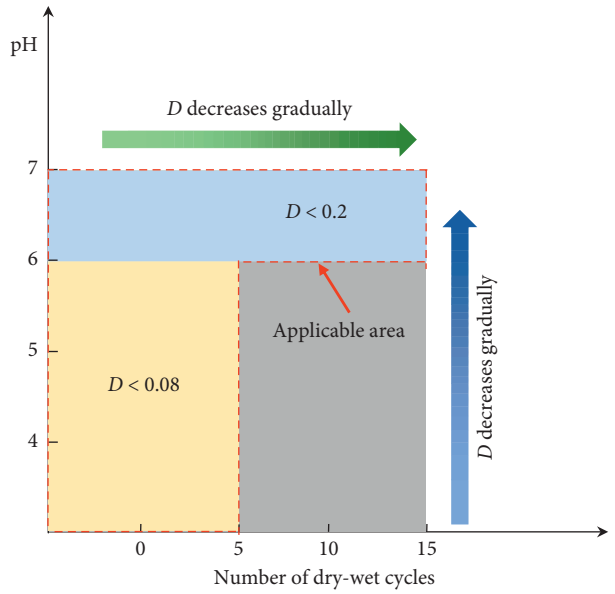

Figure 19: Schematic diagram of model application scope.

same time, when the number of dry-wet cycles is less than 5, the W value can be controlled within 0.08, which is more applicable. The specific application scope is shown in Figure 19.

Therefore, the scope of application of the model can be summarized as the case that the pH value is more than 6 in the acid solution or the number of dry-wet cycles is less than 5.

5. Conclusions

(1) In the acidic environment, with the increase in the number of cycles, the quality of the sandstone and the P-wave velocity both decrease, and the amount decreases to 0.43% and 7.87%, respectively. At the same time, with the increase of the acidic concentration, the loss of both increases. In the first three stages of the cycle, the loss of the mass and the P-wave velocity in each stage decreases gradually and then increases rapidly after 10 cycles.

(2) In an acidic environment, the peak stress and modulus of elasticity of sandstone decrease with the increase in the number of cycles, with decrease rates of 70.2% and 88.1%, respectively, whereas the peak strain increases to 55.8%, showing a softening phenomenon. The change rate of the three mechanical indicators in each stage has 10 cycles as the critical point and the change rate in Stage IV increases sharply.

(3) Microscopic analysis shows that on the one hand, acid solution will corrode rock specimens, which increases the porosity of the specimen. Microcracks begin to develop at the interface of different substances, resulting in curling of the rock particles, which decreases the physical and mechanical properties of sandstone. On the other hand, the sulfuric acid reacts with some substances inside the specimen to form precipitation, which hinders the development of pores. The phenomenon disappears gradually with the increase of the number of cycles.

(4) The damage model of uniaxial compression based on *Weibull* distribution function is established, and compared with the test results, and the model has the best effect in acid solution with less cycle times or pH value of solution greater than 6.

Data Availability

The datasets generated and analyzed during the current study are available from the corresponding author on reasonable request.

Conflicts of Interest

The authors declare that they have no conflicts of interest.

Authors' Contributions

Xin Huang and Guangchen Liu performed the experiments and analyzed the test data; Xin Huang and Yu Chen wrote the manuscript; and Jianyong Pang conceived the experiment and provided the guidance and suggestion.

Acknowledgments

The authors acknowledge the School of Civil Engineering and Architecture, Anhui University of Science and Technology, for their support to perform this research. This research was funded by the Science and Technology Project Foundation of Key Technologies for Prevention and Cure of Major Accidents in Production Safety, General Administration of State Security Supervision (No. Anhui-0003-2016AQ).

References

[1] Y. Wang, Q. Chen, Y. Y. Wei et al., "Water/rock interaction mechanism in deep-buried tunnels in karst area," *China Railway Science*, vol. 25, no. 4, pp. 55–58, 2004, in Chinese.

[2] B. Thomas, S. Radu, R. A. Kauther, and P. A. Vermeer, "A Hoek-Brown criterion with intrinsic material strength factorization," *International Journal of Rock Mechanics and Mining Sciences*, vol. 45, no. 2, pp. 210–222, 2008.

[3] C. M. Oryem, C. Riccardo, G. B. Crosta, and T. Hueckel, "Effects of mineral suspension and dissolution on strength and compressibility of soft carbonate rocks," *Engineering Geology*, vol. 184, pp. 1–18, 2015.

[4] T. Critelli, L. Marini, J. Schott et al., "Dissolution rates of actinolite and chlorite from a whole-rock experimental study of metabasalt dissolution from $2 \leq pH \leq 12$ at 25°C," *Chemical Geology*, vol. 390, pp. 100–108, 2014.

[5] Z. A. Erguler and R. Ulusay, "Water-induced variations in mechanical properties of clay-bearing rocks," *International Journal of Rock Mechanics and Mining Sciences*, vol. 46, no. 2, pp. 355–370, 2009.

[6] K. Gholamreza and A. Yasin, "Influence of wet-dry, freeze-thaw, and heat-cool cycles on the physical and mechanical properties of upper red sandstones in central Iran," *Bulletin of Engineering Geology and the Environment*, vol. 74, no. 4, pp. 1287–1300, 2015.

[7] S. Liu, G. S. Yang, and X. H. Dong, "Experimental study on influence of wetting-drying cycles on mechanical characteristics and damage of red sandstone," *Coal Science and Technology*, vol. 47, no. 4, pp. 101–106, 2019, in Chinese.

[8] Q. Y. Ma, P. Y. Yu, and P. Yuan, "Experimental study on creep properties of deep siltstone under cyclic wetting and drying," *Chinese Journal of Rock Mechanics and Engineering*, vol. 37, no. 3, pp. 593–600, 2018, in Chinese.

[9] Z. Zhou, X. Cai, L. Chen, W. Cao, Y. Zhao, and C. Xiong, "Influence of cyclic wetting and drying on physical and dynamic compressive properties of sandstone," *Engineering Geology*, vol. 220, pp. 1–12, 2017.

[10] B. Du, H. B. Bai, and G. M. Wu, "Dynamic compression properties and deterioration of red-sandstone subject to cyclic wet-dry treatment," *Advances in Civil Engineering*, vol. 2019, Article ID 1487156, 10 pages, 2019.

[11] B. Du and H. B. Bai, "A damage constitutive model of red sandstone under coupling of wet-dry cycles and impact load," *Shock and Vibration*, vol. 2019, Article ID 7692424, 12 pages, 2019.

[12] H. Y. Yao, Y. Zhu, and P. Wu, "Research on uniaxial compression and tension tests of sandstone subjected to drying-wetting cycle," *Disaster Advances*, vol. 6, no. 3, pp. 388–392, 2013.

[13] S.-C. Tang, J.-J. Wang, Z.-F. Qiu, and Y.-M. Tan, "Effects of wet-dry cycle on the shear strength of a sandstone-mudstone particle mixture," *International Journal of Civil Engineering*, vol. 17, no. 6, pp. 921–933, 2019.

[14] K. Sharma, T. Kiyota, and H. Kyokawa, "Effect of slaking on direct shear behaviour of crushed mudstones," *Soils and Foundations*, vol. 57, no. 2, pp. 288–300, 2017.

[15] W. Hua, S. Dong, Y. Li, J. Xu, and Q. Wang, "The influence of cyclic wetting and drying on the fracture toughness of sandstone," *International Journal of Rock Mechanics and Mining Sciences*, vol. 78, pp. 331–335, 2015.

[16] X. J. Yang, J. M. Wang, C. Zhu, M. He, and Y. Gao, "Effect of wetting and drying cycles on microstructure of rock based on SEM," *Environmental Earth Sciences*, vol. 78, no. 6, p. 183, 2019.

[17] H. W. Deng, S. T. Yu, and J. R. Deng, "Damage characteristics of sandstone subjected to coupled effect of freezing-thawing cycles and acid environment," *Advances in Civil Engineering*, vol. 2018, Article ID 3560780, 10 pages, 2018.

[18] S.-Q. Yang, P. G. Ranjith, H.-W. Jing, W.-L. Tian, and Y. Ju, "An experimental investigation on thermal damage and failure mechanical behavior of granite after exposure to different high temperature treatments," *Geothermics*, vol. 65, pp. 180–197, 2017.

[19] N. Li, Y. M. Zhu, S. Bo, and S. Gunter, "A chemical damage model of sandstone in acid solution," *International Journal of Rock Mechanics and Mining Sciences*, vol. 40, no. 2, pp. 243–249, 2003.

[20] N. Li, Y. M. Zhu, P. Zhang et al., "A chemical damage model of sandstone in acid environment," *Chinese Journal of Geotechnical Engineering*, vol. 25, no. 4, pp. 395–399, 2003, in Chinese.

[21] X. Liu, M. Jin, D. Li, and L. Zhang, "Strength deterioration of a Shaly sandstone under dry-wet cycles: a case study from the Three Gorges Reservoir in China," *Bulletin of Engineering Geology and the Environment*, vol. 77, no. 4, pp. 1607–1621, 2018.

[22] X. R. Liu, Z. J. Wang, Y. Fu, W. Yuan, and L. Miao, "Macro/microtesting and damage and degradation of sandstones under dry-wet cycles," *Advance in Materials Science and Engineering*, vol. 2016, Article ID 7013032, 16 pages, 2016.

[23] H. Li, Z. Zhong, X. Liu, Y. Sheng, and D. Yang, "Micro-damage evolution and macro-mechanical property degradation of limestone due to chemical effects," *International Journal of Rock Mechanics and Mining Sciences*, vol. 110, pp. 257–265, 2018.

[24] W. Yuan, X. Liu, and Y. Fu, "Study on deterioration of strength parameters of sandstone under the action of dry-wet cycles in acid and alkaline environment," *Arabian Journal for Science and Engineering*, vol. 43, no. 1, pp. 335–348, 2018.

[25] W. Yuan, X. Liu, and Y. Fu, "Chemical thermodynamics and chemical kinetics analysis of sandstone dissolution under the action of dry-wet cycles in acid and alkaline environments,"

Bulletin of Engineering Geology and the Environment, vol. 78, no. 2, pp. 793–801, 2019.

[26] Z. Wang, X. Liu, X. Yang, and Y. Fu, "An improved duncan-chang constitutive model for sandstone subjected to drying-wetting cycles and secondary development of the model in FLAC^{3D}," *Arabian Journal for Science and Engineering*, vol. 42, no. 3, pp. 1265–1282, 2017.

[27] S. Matsumoto, H. Shimada, and T. Sasaoka, "Interaction between physical and chemical weathering of argillaceous rocks and the effects on the occurrence of acid mine drainage (AMD)," *Geosciences Journal*, vol. 21, no. 3, pp. 397–406, 2017.

[28] Q. Sun and Y. Zhang, "Combined effects of salt, cyclic wetting and drying cycles on the physical and mechanical properties of sandstone," *Engineering Geology*, vol. 248, pp. 70–79, 2019.

[29] S. G. Li, R. K. Huo, B. Wang et al., "Experimental study on physicomechanical properties of sandstone under acidic environment," *Advances in Civil Engineering*, vol. 2018, Article ID 5784831, 15 pages, 2018.

[30] J. C. Fang, H. F. Deng, Y. Qi, Y. Xiao, H. Zhang, and J. Li, "Analysis of changes in the micromorphology of sandstone joint surface under dry-wet cycling," *Advances in Materials Science and Engineering*, vol. 2019, Article ID 8758203, 11 pages, 2019.

[31] X. Yang, J. Wang, D. Hou, C. Zhu, and M. He, "Effect of dry-wet cycling on the mechanical properties of rocks: a laboratory-scale experimental study," *Processes*, vol. 6, no. 10, p. 199, 2018.

[32] H. Ni, L. Zhang, D. Zhang, X. Wu, and X. Fu, "Weathering of pisha-sandstones in the wind-water erosion crisscross region on the LOESS PLAteau," *Journal of Mountain Science*, vol. 5, no. 4, pp. 340–349, 2008.

[33] C. Zhang, Z. Y. Cai, Y. H. Huang, and H. Chen, "Laboratory and centrifuge model tests on influence of swelling rock with drying-wetting cycles on stability of canal slope," *Advances in Civil Engineering*, vol. 2018, Article ID 4785960, 10 pages, 2018.

[34] M. Hu, Y. Liu, J. Ren, R. Wu, and Y. Zhang, "Laboratory test on crack development in mudstone under the action of dry-wet cycles," *Bulletin of Engineering Geology and the Environment*, vol. 78, no. 1, pp. 543–556, 2019.

[35] ISRM, *The Complete ISRM Suggested Methods for Rock Characterization, Testing and Monitoring*, R. Ulusay and J. Hudson, Eds., International Society for Rock Mechanics, Salzburg, Austria, 2007.

[36] Y. Chen, L. Zhang, H. Xie, J. Liu, H. Liu, and B. Yang, "Damage ratio based on statistical damage constitutive model for rock," *Mathematical Problems in Engineering*, vol. 2019, Article ID 3065414, 12 pages, 2019.

[37] B. C. Yang, L. Xue, and M. M. Wang, "Evolution of the shape parameter in the Weibull distribution for brittle rocks under uniaxial compression," *Arabian Journal of Geosciences*, vol. 11, no. 12, Article ID 321, 2019.

[38] H. X. Gao and K. L. Yin, "Discuss on the correlations between landslides and rainfall and threshold for landslide early-warning and prediction," *Rock and Soil Mechanics*, vol. 28, no. 5, pp. 1055–1060, 2007, in Chinese.